JACS
JOURNAL OF THE AMERICAN CHEMICAL SOCIETY
pubs.acs.org/JACS
Article

Mechanistic Elucidation of the Hula-Twist Photoreaction in Hemithioindigo

Tobias Fischer,[⊥] Jonas Leitner,[⊥] Aaron Gerwien,[⊥] Peter Mayer, Andreas Dreuw,* Henry Dube,* and Josef Wachtveitl*

Cite This: J. Am. Chem. Soc. 2023, 145, 14811−14822
Read Online
ACCESS | Metrics & More | Article Recommendations | Supporting Information

ABSTRACT: The Hula-Twist (HT) photoreaction represents a fundamental photochemical pathway for bond isomerizations and is defined by the coupled motion of a double bond and an adjacent single bond. This photoreaction has been suggested as the defining motion for a plethora of light-responsive chromophores such as retinal within opsins, coumaric acid within photoactive yellow protein, or vitamin D precursors, and stilbenes in solution. However, due to the fleeting character of HT photoproducts a direct experimental observation of this coupled molecular motion was severely hampered until recently. To solve this dilemma, the Dube group has designed a molecular framework able to deliver unambiguous experimental evidence of the HT photoreaction. Using sterically crowded atropisomeric hemithioindigo (HTI) the HT photoproducts are rendered thermally stable and can be observed directly after their formation. However, following the ultrafast excited state process of the HT photoreaction itself has not been achieved so far and thus crucial information for an elementary understanding is still missing. In this work, we present the first ultrafast spectroscopy study of the HT photoreaction in HTI and probe the competition between different excited state processes. Together with extensive excited state calculations a detailed mechanistic picture is developed explaining the significant solvent effects on the HT photoreaction and revealing the intricate interplay between productive isomerizations and unproductive twisted intramolecular charge transfer (TICT) processes. With this study essential insights are thus gained into the mechanism of complex multibond rotations in the excited state, which will be of primary importance for further developments in this field.

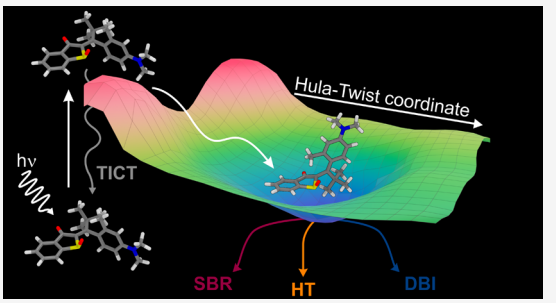

INTRODUCTION

In recent years, the class of hemithioindigo (HTI) photoswitches has gathered attention based on a multitude of favorable properties such as high thermal bistability, fatigue-resistant switching, and light responsiveness in the visible spectral region.[1−6] These properties allow for various applications in the fields of biological chemistry,[7−10] supramolecular chemistry,[11−14] and molecular machines.[15]

Apart from these applications, HTIs have also been used as model systems to study light-induced reaction mechanisms.[4,16−19] Upon illumination, HTIs typically undergo double bond isomerization (DBI) within a few fs to ps. However, depending on the substitution pattern and solvent polarity, the formation of twisted intramolecular charge transfer (TICT) states associated with single bond twisting (SBT) can be observed as an alternative deactivation channel (Scheme 1).[18,19]

TICT formation can be induced by introducing a pretwist into the single bond adjacent to the central double bond as well as electron-donating substituents at the stilbene moiety. The ratio of SBT via TICT vs DBI can then be controlled by the polarity of the solvent, where high polarity favors the SBT/TICT pathway nearly abolishing DBI and low polarity entirely eliminates SBT/TICT favoring very efficient DBI.[18]

To evidence other possible photochemical bond rotations, the Dube group developed the synthesis of double bond substituted HTIs[20] and sulfur oxidized HTIs (Scheme 1b).[21] By combining these two substitution patterns, it was possible to create derivatives containing a significantly pretwisted single bond, which cannot rotate easily in the ground state because of very strong steric hindrance. If this twisted stilbene fragment is additionally rendered nonsymmetric by different *ortho*-substituents such as in derivative **1** (Scheme 1 and Figure 1), atropisomers can be distinguished as diastereomers in these structures. In total, four diastereomers can be isolated at ambient temperatures for structures like **1** and three different isomerization reactions are possible for each of them. The first one is the long known DBI, the second is a full single bond

Received: April 5, 2023
Published: June 26, 2023

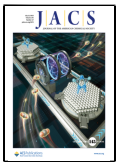

Scheme 1. Different Photoreactions Executed by the Hemithioindigo (HTI) Photoswitch: (a) Two Previously Evidenced Photoreactions of HTIs, DBI (top) and SBT/TICT Formation; (b) Hula-Twist (HT) and SBR as Additional Photoreactions That Can Be Evidenced for Sterically Hindered Sulfoxide HTI Derivatives[a]

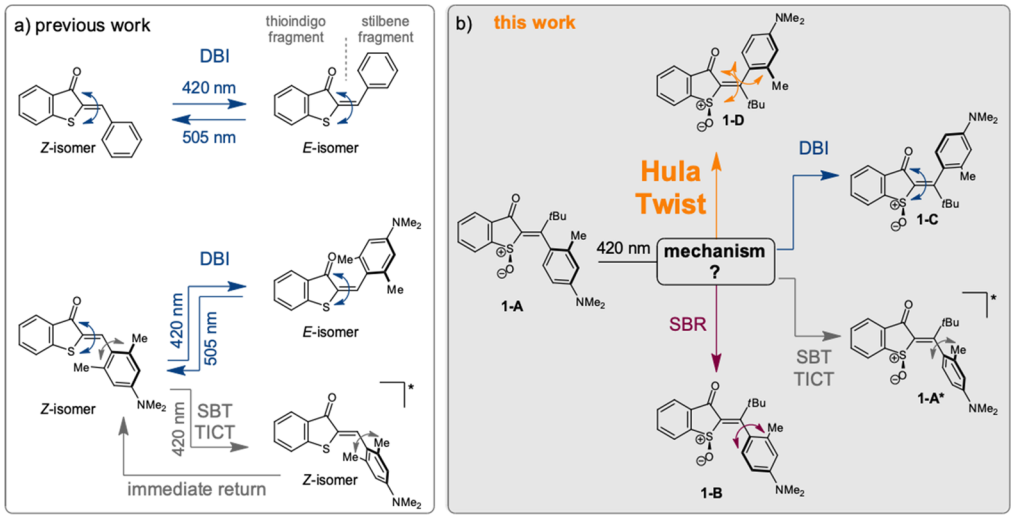

[a]The molecular structure of HTI **1** was used for elucidation of the excited state mechanism in the present study.

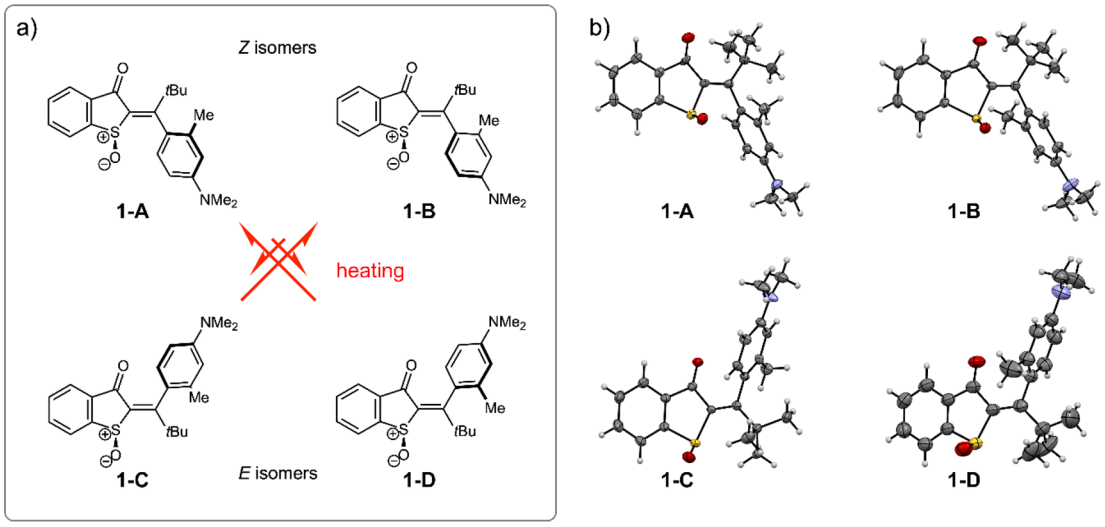

Figure 1. Structures of **1-A** to **1-D** and their thermal conversions. (a) Schematic representations of the four diastereomers of HTI **1** (only enantiomers with (*S*)-configured sulfoxide stereo center are shown. Thermal conversions occur selectively as HT processes between **1-A** and **1-D** as well as **1-B** and **1-C**. (b) Structures of **1-A** to **1-D** in the crystalline state.

rotation (SBR – note that this motion is different from the SBT, as in the latter case no full rotation but rather a twist is executed), and the third is a combined DBI and SBR process also known as Hula-Twist (HT).[22−24] With a molecular setup similar to **1** it was possible to provide a first direct experimental evidence for the HT isomerization and in addition demonstrate significant influences of solvent polarity, viscosity, and temperature on this photoreaction.[17] Since then, the HT photoreaction was applied in the construction of new archetypes of molecular machines, such as photon-only driven motors,[25] or multistate photoswitch architectures that allow high-state densities and extremely selective sequential switching processes.[26] These examples already highlight the immense potential of novel photoreactions for the construction of smart and responsive molecular systems.

Despite the progress, conscious design and rational tailoring of HT photoreactions are currently out of reach as no detailed mechanistic understanding is available. Earlier attempts at mechanism elucidation in e.g. stilbene[23,27] and vitamin-D precursors[28,29] were hampered by the ambiguity of different possible and overlapping photoreactions and no direct evidence of the HT photoreaction itself.[30−32] Similarly, HT photoreactions are also disputed for biologically relevant chromophores such as *p*-coumaric acid.[33−35] The particular HTI molecular setup allows direct study of the mechanism, dynamics, and environmental influences of the HT photoreaction as well as the competition of HT with DBI and SBR pathways. It thus represents an ideal molecular framework to gain deep knowledge about an intricate and fundamental photoreaction and its mechanism.

In this work, we present a combined ultrafast UV/vis spectroscopic and quantum chemical investigation to elucidate the contribution of HT and other photoreaction mechanisms within a novel donor-substituted HTI photoswitch. We reveal

https://doi.org/10.1021/jacs.3c03536
J. Am. Chem. Soc. 2023, 145, 14811−14822

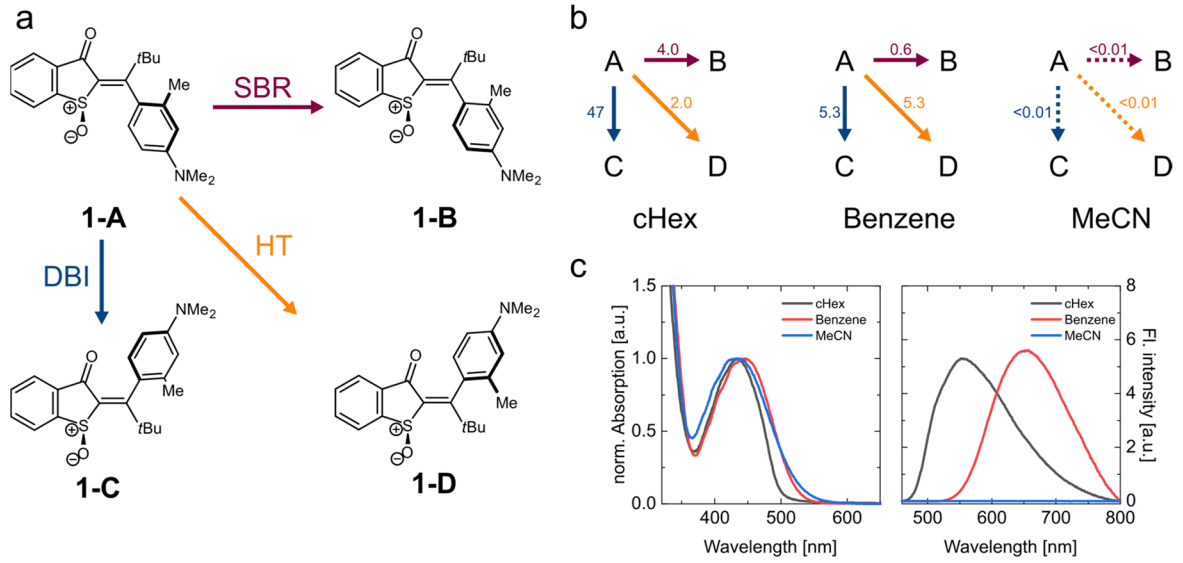

Figure 2. Schematic representation of possible productive photochemical reaction pathways in HTI **1-A**. (a) Schematic representation of the four possible diastereomers (**1-A** to **1-D**), where **1-A** and **1-B** are *Z*-isomers and **1-C** and **1-D** *E*-isomers. Isomer **1-A** can be converted to **1-B** via SBR, to **1-C** via DBI, or to **1-D** via HT. (b) Quantum yields for the individual photoreactions of **1-A** determined in solvents of different polarity (cyclohexane (cHex), benzene and acetonitrile (MeCN)). Dashed arrows indicate quantum yields <0.01%. (c) Normalized absorption (left) and fluorescence spectra (right) of isomer **1-A** in different solvents. Fluorescence spectra were recorded after excitation at 460 nm.

the overall photodynamics, identify competing excited state pathways, and test for environmental influences on the photoreactions. We further discuss whether HT and DBI occur on separate pathways or branch from a common pathway on the excited state surface.

EXPERIMENTAL SECTION

Sample Preparation. The investigated compound **1-A** was dissolved in the respective solvent and diluted appropriately. For steady state and transient absorption measurements (1 mm cuvette) optical densities (OD) of roughly 0.5 at 460 nm were used in acetonitrile (MeCN) and benzene solution while in cyclohexane (cHex) solution an OD of 0.3 was used due to limited solubility. For the fluorescence measurements (1 cm cuvette) an OD of 0.1 at 460 nm was used.

Spectral Characterization. Absorption spectra were recorded on a Specord S600 absorption spectrometer (Analytik Jena). Fluorescence spectra were obtained on an FP 8500 fluorimeter (Jasco) with excitation at 460 nm. The recorded fluorescence spectra were corrected for reabsorption, background, nonlinearity of detector sensitivity for different wavelengths, excitation intensity, and solvent fluorescence.

Quantum Yield Determination. See Supporting Information (SI) for details.

Transient Absorption (TA). Time-resolved transient absorption (TA) measurements were performed using a home-built pump–probe setup described previously in detail.[36] In summary, ultrashort laser pulses (1 mJ, 775 nm, 130 fs, 1 kHz) used for pump and probe generation were provided by a Ti:Sa amplifier system (Clark, MXR-CPA-iSeries). Pump pulses were generated using a home-built two stage NOPA (noncollinear optical parametric amplifier). To obtain short pulses a prism compressor was used and placed between the two NOPA stages. To generate the probe pulses the laser fundamental was focused into a continuously moving CaF_2 crystal (5 mm). The probe pulses were then split into probe and reference beam. The reference beam was guided directly into a spectrograph (AMKO Multimode), while the probe beam was focused at the sample position, collected, and directed into a second spectrograph. The spectrographs contained gratings with 600 grooves/mm blazed at 500 nm and a photodiode array with a detection range of 360 to 720 nm. Anisotropic contributions were eliminated by measuring under magic angle conditions (54.7° pump–probe polarization difference). The experiments were carried out in a fused silica cuvette with a 1 mm optical path length, which was constantly moved in the plane perpendicular to the pump pulses to avoid accumulation of photoproducts. In the experiments conducted in this work, pump energies of 90 nJ/pulse were used since higher energies induced multiphoton effects in benzene, which led to mixed dynamics. For similar reasons the excitation wavelength was not shifted further into the UV toward the maximum of the observed absorption bands.

Data Analysis. Data analysis was performed using OPTIMUS (www.optimusfit.org).[37] We applied global target analysis (GTA) using a sequential model (A → B → C → ···) to adequately fit the data. Aside from the decay-associated spectra (DAS) routinely obtained in global lifetime analysis, GTA yields the so-called evolution-associated difference spectra (EADS), which contain spectral information on the states present in the kinetic model.

Computational Details. All quantum chemical calculations were performed using Gaussian 16[38] unless mentioned otherwise. The ground state structures were optimized with density functional theory (DFT)[39] using the CAM-B3LYP[40] exchange-correlation (xc) functional and def2-SVP basis set. Solvent effects were included through the integral equation formalism (IEF) of the polarizable continuum model (PCM).[41] The dielectric and optical dielectric constants of all studied solvents are listed in Table S3 in the SI. Linear-response time-dependent DFT (TD-DFT)[42] was employed for the calculation of absorption spectra and excited states properties using the same xc-functional/basis set combination. Excited state geometry optimizations of the first excited singlet state S_1 were performed to investigate the influence of solvent effects on the emission energy. The *Z*/*E* isomerization is further studied by means of one-dimensional relaxed scans along the isomerization coordinate represented by the marked dihedral angle in Figure 5. In general, solvent effects were included in excited state calculations by means of the linear-response (LR-) PCM formalism, while single-point energies at specific equilibrium geometries of the S_0 and the S_1 states, for example, were further calculated using the state-specific (SS-) PCM formulation.

Further investigations of relaxation pathways involving S_0/S_1 conical intersections (CI) were performed using Q-Chem 5.2.[43] Spin-flip DFT (SF-DFT)[44] has been employed for optimizations of the minimum energy crossing points (MECP) using the CAM-B3LYP/def2-SVP xc-functional/basis set combination and the conductor like polarizable continuum model (C-PCM). Thereby

https://doi.org/10.1021/jacs.3c03536
J. Am. Chem. Soc. 2023, 145, 14811−14822

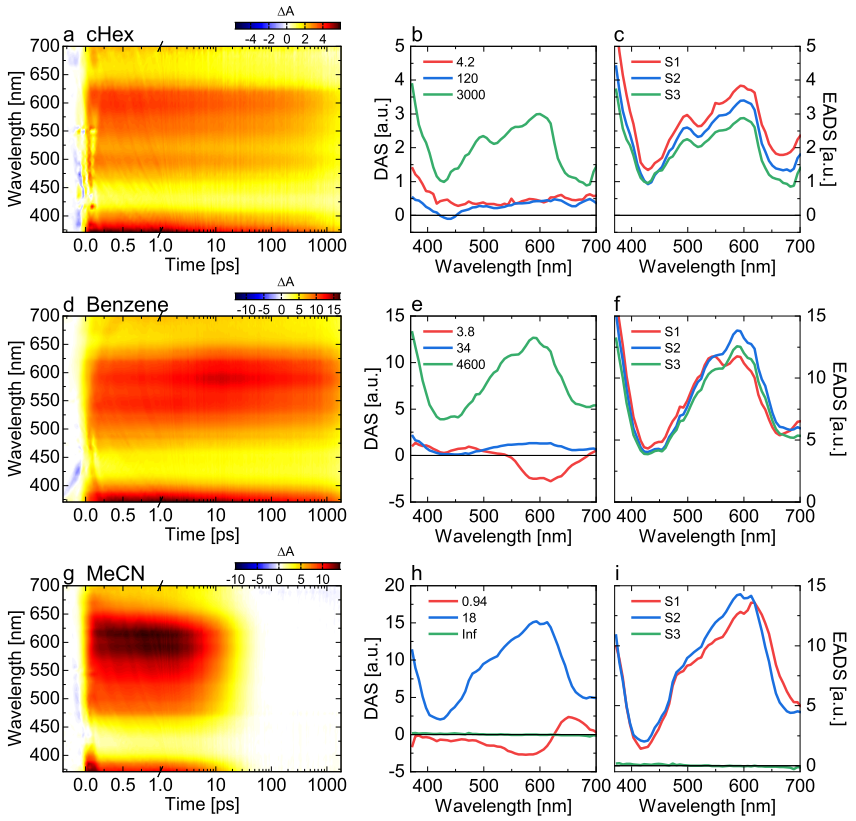

Figure 3. Ultrafast excited state dynamics of **1-A** after excitation at 460 nm in cHex (a,b,c), benzene (d,e,f), and MeCN (g,h,i). (a,d,g) Transient absorption spectra of **1-A**. Red indicates positive signals of ESA and product absorption (PA), while negative signals can be assigned to leftover contributions of a coherent artifact. (b,e,h) Decay-associated spectra (DAS) and (c,f,i) evolution-associated difference spectra (EADS) obtained from the respective global target analysis of (a,d,g). Note that the first sub-100 fs lifetime was omitted in all data sets due to limited time resolution caused by a complex and strong coherent artifact.

two CIs have been optimized along the previously determined isomerization coordinate. Note that the Tamm–Dancoff approximation (TDA)[45] was applied.

RESULTS AND DISCUSSION

Synthesis of 1. The synthesis of **1** follows an established protocol reported earlier.[20] It starts from commercially available thiosalicyclic acid (**2**) and α-bromo-ketone **3**. After a nucleophilic substitution reaction, the corresponding thioether **4** is obtained in 98% yield. Base addition leads to formation of the hydroxyl-HTI **5** in 97% yield. Chlorination using thionyl chloride gives the chlorinated HTI **6** quantitatively, which was then cross-coupled with boronic acid **7** to give double-bond substituted HTI **8**. A final oxidation of the sulfur to the corresponding sulfoxide yields HTI **1** again in very good yield.

Properties of HTI 1. HTI **1** can assume four diasteromeric states **1-A** to **1-D** (Figure 1a), which are thermally stable at ambient conditions. Each of these can assume two enantiomeric forms depending on the configuration at the sulfoxide stereo center. For clarity we only show the enantiomers with (*S*) configured sulfoxide, although racemic mixtures were studied here.

All four diastereomers **1-A** to **1-D** were separated, and crystals suitable for X-ray structural analysis were obtained for enantiopure **1-A**-(*S*) and **1-B**-(*S*) as well as for racemic **1-C** and **1-D** (Figure 1b), which allowed direct assignment of spectra to a particular diastereomer.

Investigation of the thermal behavior revealed very selective interconversions between isomers of HTI **1**. At elevated temperatures of 80 °C combined double and single bond rotations (i.e., HT) occur as thermal isomerization reactions interconverting only **1-A** and **1-D** or **1-B** and **1-C**. For each interconverting pair the *Z* configured isomers are thermally the most stable (i.e., **1-A** and **1-B**), but an appreciable amount of the *E* configured isomers is present in thermal equilibrium in both cases (for more details and quantitative numbers see the Supporting Information).

Steady State Properties of 1-A. To understand the photophysical properties of sterically restricted HTI **1**, steady state absorption and fluorescence spectra were measured as well as the photoisomerization quantum yields of isomer **1-A** in different solvents (see Figure 2 and Supporting Information). Isomer **1-A** was chosen for this study, as it undergoes pronounced HT photoreactions upon irradiation, the relative propensity of which can be modulated strongly by solvent polarity. Thus, the process of HT can be studied most conveniently for this isomer without the need to resort to low temperature experiments.

In cHex, isomer **1-A** exhibits its main absorption peak at 433 nm, which is slightly red-shifted and broadened in more polar solvents. The bathochromic shift in benzene amounts to 13 nm while in more polar solvents like CH_2Cl_2, DMSO, or MeCN no further red-shifting but instead broadening is observed, indicating only a small influence of the polarity on the $S_0 \rightarrow S_1$ gap. In contrast, the fluorescence is significantly more solvent dependent (see Figure 2c and the Supporting Information for

https://doi.org/10.1021/jacs.3c03536
J. Am. Chem. Soc. 2023, 145, 14811−14822

further details). In cHex, the fluorescence maximum is located at 550 nm showing a large Stokes shift of ∼120 nm. With increasing solvent polarity, the fluorescence undergoes a large bathochromic shift of >100 nm in benzene and >200 nm in CH_2Cl_2 before disappearing completely in the very polar MeCN. In DMSO, a possible dual fluorescence could be present. This behavior is similar to other amine-donor substituted and twisted HTIs where the fluorescence is believed to be quenched by a strongly stabilized conical intersection of a TICT state with the ground state in polar environments.[19]

Upon illumination with blue light, photoconversion of isomer **1-A** to the two *E*-isomers **1-C** and **1-D** and the *Z*-isomer **1-B** are observed by NMR spectroscopy in apolar solvents. Using UV/vis spectroscopy, no distinction between the two atropisomers of either *E* or *Z* configuration is possible because of their very similar spectra and only the sum amount of formed *E*-isomer can be estimated. Productive photoisomerization of **1-A** decreases with increasing polarity of the solvent and is completely abolished in MeCN. Precise determination of the photoreaction quantum yields with NMR spectroscopy revealed more details on the influence of solvent polarity on the individual reaction pathways, as all isomers **1-A** to **1-D** can be distinguished with this method. In cHex, DBI is the most pronounced pathway with a 47% quantum yield while SBR and HT are less pronounced with 4% and 2%, respectively. However, already in the slightly more polar benzene the DBI quantum yield is reduced to only 5%, while the SBR vanishes almost completely. Interestingly, the proposed HT pathway is significantly less affected by the solvent change, which leads to a situation in which DBI and HT possess similar quantum yields. A further increase of polarity to CD_2Cl_2/CH_2Cl_2 or MeCN abolishes any form of photoproduct formation while also fluorescence is quenched entirely. Similar solvent polarity dependencies of the product formation quantum yield have been observed in other HTIs, especially in pretwisted systems.[18,19]

Ultrafast Dynamics of 1-A. To obtain a dynamic picture of the excited state behavior of **1-A**, we performed ultrafast transient absorption measurements in cHex, benzene, and MeCN solutions (Figure 3). In all measurements, only positive signals are observed, which can be assigned to excited state absorption (ESA). The small negative signals at times <100 fs in all solvents can be assigned to a coherent artifact, which could not be removed completely. Surprisingly, no ground state bleach (GSB) or stimulated emission (SE) signals were observed, which are most likely overcompensated by the strong ESA signals. The ESA signals in cHex and benzene persist until the end of the time range of our experiments showing a very long-lived excited state (Figure 3a,d), while in MeCN the excited state is shorter lived decaying completely within 30 ps (Figure 3g). The short lifetime in MeCN is in good agreement with the drastically reduced fluorescence observed in the stationary experiments.

We performed global target analysis applying a sequential model to uncover further details of the excited state dynamics (Figure 3 b,c,e,f,h,i). In cHex, the first lifetime component at 4.2 ps shows an overall decrease of the ESA (Figure 3b). This could be assigned to an initial decay of the excited state or alternatively to solvent reorganization. A similar low ps lifetime can be observed in both benzene and MeCN with 3.8 and 0.9 ps, respectively, but with different spectral signatures, which is most likely due to the different electrostatic properties of the three solvents. Considering the presence of such a component in all three solvents this lifetime is most likely due to solvent reorganization. The necessity of solvent reorganization occurring on the excited state surface is based on the considerable difference in polarity of **1-A** between ground and excited state. This becomes evident by the different shifting behavior of absorption and fluorescence upon changing the solvent polarity.

At later times, a second lifetime component of 120 and 34 ps, respectively, can be observed in both cHex and benzene showing a positive amplitude in the DAS < 420 nm and >450 nm indicating a decay or change in extinction coefficient of the ESA and potentially a ground state recovery. Due to significant overlap of the strong ESA signal, the ground state absorption of isomer **1-A**, and the photoproducts, it is challenging to assign photoproduct formation to this step. If this process was related to ESA decay, a prior excited state branching would be required yielding a second excited state population with the same absorption profile, which is quite unlikely. Note, additionally, that the small amplitude compared to the following main excited state decay indicates that this cannot be the main productive channel for the *Z*/*E* isomerization. In such case, a significantly larger amplitude would be expected in cHex compared to the amplitude of the main excited state decay because of the high DBI quantum yield in this solvent. Hence, it is more plausible that this process is related to relaxation in the excited state or further solvent reorganization modulating the extinction of the excited state and in turn the amplitude of the ESA.

The excited state then decays on a much longer time scale where the decay occurs later in benzene than in cHex as readily observable by the higher amplitude of the ESA at long delay times. Consequently, the kinetic analysis yields lifetimes of 3.0 ns in cHex and ∼4.6 ns in benzene. In contrast, in the polar MeCN an overall excited state lifetime of only 18 ps was observed. Thus, there is an interesting behavior established for the overall excited state lifetime maximum, when changing the polarity of the solvent. First, the excited state lifetime increases upon increasing the polarity from cHex to benzene, but when moving to the very polar MeCN the lifetime is shortened significantly (Figure 3g,h,i). This contrasts the behavior in many photoswitches and most HTIs, where only a continuous trend is seen when increasing solvent polarity.

Such discontinuity typically signifies a change of mechanism and a change of photoreactive pathways (for a related discontinuity of the excited state mechanism in response to systematic substituent changes, see ref 5). In twisted HTIs bearing strong donor groups, a similar maximum behavior in terms of excited state lifetimes as well as a significant decrease in photoisomerization quantum yield in response to increasing solvent polarity is observed. This behavior could be associated with a second deexcitation pathway via a TICT state, which competes with the DBI pathway starting from an initial excited state $S_{1,min}$.[18,19] In another study, planar HTIs were reported to show a continued increase in excited state lifetime and fluorescence intensity with increasing solvent polarity. In that case, the barrier in the excited state increased due to stabilization of the prior polar S_1 minimum ($S_{1,min}$) but TICT formation was not observed due to a lack of pretwisting in the ground state.[46] For HTI **1-A**, we observe a behavior more similar to twisted HTIs with the excited state lifetime first increasing, then decreasing with rising solvent polarity.

https://doi.org/10.1021/jacs.3c03536
J. Am. Chem. Soc. 2023, 145, 14811−14822

Apart from the different excited state lifetimes, the overall dynamics are similar in all three solvents with different degrees of solvent reorganization followed by excited state decay. Additionally, throughout all measurements the spectral shape of the ESA itself remains rather similar despite the significant change in excited state lifetime and product ratios. This behavior rules out the occurrence of completely separate reaction pathways for the individual reaction processes like SBR or DBI. In such a case, a significant difference in the shape of the ESA would have been expected for HTI **1-A** in benzene and cHex based on the significant reduction in population of the DBI pathway. Therefore, it seems that all photoproducts are generated on a shared pathway, or the distinctions can only be observed on the ns-time scale outside our measurement window. This contrasts with other HTIs where a clear spectral separation into a TICT/SBT pathway and a DBI pathway is observed.[18,19]

Based on these findings a preliminary model can be constructed. With the long-lived excited state in benzene and cHex, a significant barrier is expected on the excited state surface for productive photoreactions, which increases at first with rising polarity. This is in good agreement with the observed red shift in the fluorescence, indicating that the $S_{1,min}$ state, formed after excitation and before passing the barrier, is likely stabilized in polar conditions similar to a previously proposed model.[46] To accommodate for the decrease in lifetime and quantum yield, an additional pathway draining the $S_{1,min}$ population has to be present at higher polarity of the solvent. We can further characterize this pathway based on the observation that the spectral shape of the ESA is only weakly solvent dependent and does not change significantly during the photoreaction. Therefore, the additional pathway must originate from the same $S_{1,min}$. Otherwise, a different state with identical ESA features generated by excited state branching would have to be present, which is unlikely. To further support and refine our model, we performed ground and excited state quantum chemical calculations to identify the specific reactive pathways.

Quantum Chemical Calculations. In a first step, we calculated the $S_0 \rightarrow S_1$ vertical excitation energies of **1-A** at its ground state equilibrium geometries (Table 1). All energetically higher excited states do not play a role in the investigated isomerization mechanism. Within the expected accuracy of our calculations, the results agree well with the experimental absorption bands and show only a small dependence on the solvent polarity. The natural transition orbitals (NTO) calculated without a solvation model are shown in Figure 4, and the static dipole moments of S_1 are listed in Table 1, which allow for a judgment of the charge transfer (CT) character of the S_1 state. Indeed, S_1 possesses CT character: electron density is transferred from the stilbene fragment to the thioindigo fragment. Furthermore, S_1 can be identified as a TICT state, which is already present at the Franck−Condon (FC) geometry, due to the strong pretwisting of **1-A**. In contrast, previous calculations on unsubstituted HTI identified S_1 to be of $\pi\pi^*$ character,[4,46,47] while the corresponding TICT state is reached via a competing relaxation channel that renders the DBI less productive.[18]

Table 1. Excitation Energy ω and Dipole Moment μ for the Excited S_1 State Computed at the Ground State ($S_{0,min}$; the FC Geometry) and S_1 ($S_{1,min}$) Equilibrium Geometries at TD-DFT/CAM-B3LYP/def2-SVP/SS-PCM Level of Theory[a]

	$S_{0,min}$/FC geometry		$S_{1,min}$ geometry		Excess energy
	ω_1 [eV]	μ_1 [D]	ω_1 [eV]	μ_1 [D]	$E_{1,S0,min} - E_{1,S1,min}$ [eV]
gas phase	3.36	12.9	2.60	15.9	0.33
cHex	2.55	20.5	1.96	18.9	0.20
benzene	2.44	20.9	1.86	19.3	0.20
MeCN	2.57	20.5	0.52	23.4	1.32

[a]Additionally, the difference in the absolute energies of the S_1 state at $S_{0,min}$ and $S_{1,min}$ configuration, the excess energy, is given.

This difference in excited state character is a consequence of the electron-donating substituents on the stilbene fragment and the oxidation of the sulfur on the thioindigo part, which increases the electron-donating and -accepting capabilities of the stilbene and thioindigo fragments, respectively. Altogether, this stabilizes the CT state as S_1, and thus isomer **1-A** is initially excited into S_1, which has strongly pronounced CT character.

In a next step, the equilibrium geometry of the S_1 state has been optimized starting at the FC geometry, i.e., the equilibrium geometry of the ground state. However, the structure of **1-A** changes only slightly during this geometry optimization. Therefore, the experimentally observed strong Stokes shift in polar solvents is most likely dominated by the CT and the subsequent relaxation of the surrounding solvent molecules rather than by exhaustive structural relaxation of **1-A** itself. The corresponding calculated emission energies from the S_1 minimum are listed in Table 1. In contrast to the absorption energies, the fluorescence energies show a strong dependence on the solvent polarity: the S_1 emission energies decrease strongly with increasing solvent polarity. This is a consequence of the strong stabilization of the polar S_1 CT state in polar environments, which reproduces the experimentally observed red shift of the fluorescence qualitatively. Only state-specific (SS) PCM is capable of correctly reproducing this trend, while LR-PCM only yields a minor red shift below 0.1 eV comparing cHex and MeCN, since SS-PCM is able to capture the strong response of the solvent to the CT excitation. Therefore, the stabilization of the polar S_1 state is much stronger with SS-PCM than with LR-PCM.[48] However, these results emphasize the importance of performing additional SS-PCM single point calculations to improve the description of the CT S_1 state.

A first preliminary explanation for the reduced excited state lifetime in polar environments can already be given: due to the increasing difference between the S_1 energies at the FC geometry and the S_1 equilibrium geometry, $E_{1,S0,min} - E_{1,S1,min}$, more excess energy is available in polar solvents once the S_1 equilibrium structure is reached. In other words, the S_1 state is more strongly vibrationally excited, i.e., simply hotter. Simultaneously, the S_0 and S_1 states approach each other in the $S_{1,min}$ region strongly hinting at a spatially close-by conical intersection, which should become more accessible in polar solvents due to the significantly higher excess energy. This generally leads to an acceleration of the radiation-less relaxation with increasing solvent polarity.

To further investigate the *Z*/*E*-isomerization of **1-A**, the energetically most favorable isomerization pathway starting from the S_1 *Z*-minimum has been calculated using LR-PCM for one apolar solvent, i.e., benzene, and one polar solvent, i.e., MeCN. Therefore, relaxed scans along the central dihedral angle of **1-A** have been computed by fixing the angle to a

https://doi.org/10.1021/jacs.3c03536
J. Am. Chem. Soc. 2023, 145, 14811−14822

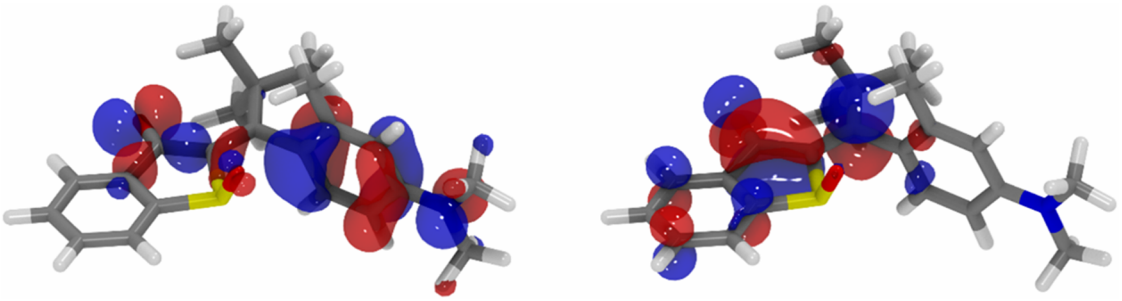

Figure 4. Highest occupied (left) and lowest unoccupied (right) NTO for S_1 of **1-A** in the gas phase with an isovalue of 0.035.

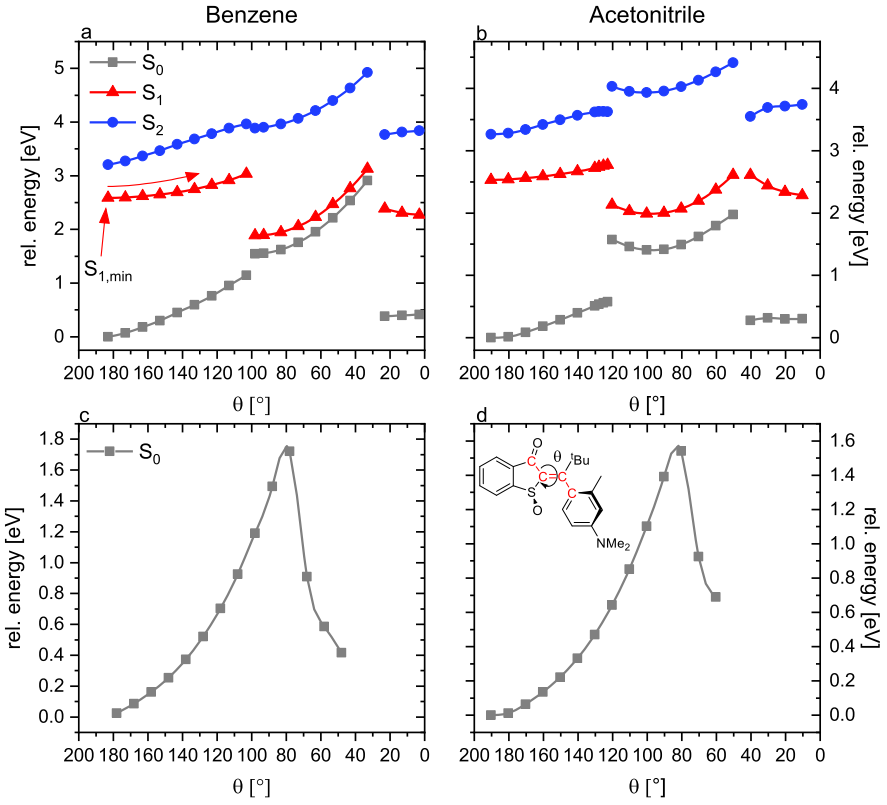

Figure 5. Relaxed one-dimensional scans of the PES of **1-A** leading to **1-D** along the dihedral angle θ (marked red in the inset). In the upper row (a,b), the S_1 relaxed scans are shown, while in the lower row (c,d) the relaxation has been calculated in the electronic ground state. Note that these correspond to two different reaction coordinates although the same dihedral angle θ has been scanned, therefore the ground state energies differ in the upper and lower panels. For the scans in the left column (a,c) a PCM for benzene has been employed, while for the right column (b,d) one for MeCN has been used.

constant value between 190° and 0° and allowing all other nuclear coordinates to relax freely. The one-dimensional PES cuts are shown in Figure 5. In Figure 5a and b, the S_1 state is relaxed; i.e., a S_1 minimum energy path is depicted along with the corresponding ground state energies. In Figure 5c and d, the S_0 state is structurally relaxed, these curves thus display a thermal isomerization path in the ground state. Hence, the pathways in Figure 5a,b and Figure 5c,d describe generally different isomerization pathways with different ground state energies. Analysis of the nuclear motions along these relaxed scans reveals an HT isomerization mechanism; i.e., HT is energetically more favorable than the exclusive DBI for the *Z*/*E*-isomerization, in both the ground and excited state. The sterically demanding substituents hinder *Z*/*E*-isomerization via DBI, since the methyl group on the stilbene fragment is clamped between the two oxygens of the thioindigo fragment, which immediately leads to a corotation of the phenyl ring when rotating around the central double bond.

The relaxed scans in the S_1 state (Figure 5a and b) feature similar shapes in MeCN and benzene: starting from the S_1 minimum of the *Z*-isomer **1-A** on the left, an isomerization barrier must be passed, which depends on the solvent polarity. The barrier height in benzene is 0.45 eV, while in MeCN a smaller barrier of 0.25 eV is found when the LR-PCM formalism is applied. However, the barrier heights drastically increase to 0.94 and 1.54 eV in benzene and MeCN, respectively, if the more reliable SS-PCM is applied, i.e., the barrier now grows with increasing solvent polarity, which agrees well with the experimentally observed decreasing quantum yield in more polar solvents. The increasing barrier height can be explained by means of the stabilization of the polar S_1 state: the S_1 minimum is more strongly stabilized than

https://doi.org/10.1021/jacs.3c03536
J. Am. Chem. Soc. 2023, 145, 14811−14822

the maximum of the barrier, as indicated by the lower dipole moments of 11.6 and 13.5 D in benzene and MeCN, respectively. Recalling the previously discussed excess energies of 0.20 eV in benzene and 1.32 eV in MeCN, the energy in both solvents is insufficient to cross the isomerization barrier easily. However, in MeCN only 0.22 eV is missing making it more likely to pass the barrier, while in benzene most of the population is trapped in the S_1 minimum.

At dihedral angles θ = 120° and 100° in MeCN and benzene, respectively, an S_0/S_1 conical intersection is passed, which leads to the observed discontinuities in the one-dimensional cut through the PES. By inspection of the state dipole moments, it becomes evident that S_0 and S_1 have interchanged, i.e., in the central parts of the scans at dihedral angles θ between 50° and 120° in MeCN and 30° and 100° in benzene, the initially excited CT state has become the ground state. In other words, in this region of the PES, the ground state can be assigned as the TICT state. Thus, the seeming discontinuities arise from the change of the optimized state and the resulting structural modifications. In particular, the carbonyl oxygen can now pass a methyl group of the *tert*-butyl group due to the constrained dihedral angle. Together, the sudden concomitant changes of electronic and geometric structure of S_1 explain the discontinuity of the energy in the one-dimensional representation of Figure 5a and b. Note that the second discontinuity at lower dihedral angles can be explained similarly. In the central part of the relaxed scans between the two discontinuities in Figure 5b, it is suggestive that a stable ground state TICT equilibrium structure should exist in MeCN. However, this is not the case, since unconstrained ground-state geometry optimizations starting at these structures have always led back to the minima of the apolar ground state. On the contrary, the S_1 state, which is the non-CT state in this PES region, possesses an excited-state equilibrium structure at a dihedral angle of 97° in MeCN and 98° in benzene.

Overall, S_0 and S_1 possess a similar shape in the central part of the relaxed S_1 scan and are energetically separated by only a small energy gap. This suggests that an S_0/S_1 CI may be spatially close. Therefore, we validated the TD-DFT results by recalculating the relaxed scans with SF-DFT (Figure S56 in the SI), which can generally better cope with such multiconfigurational situations. Indeed, SF-DFT reproduces the TD-DFT results qualitatively. In addition, a minimum-energy crossing point (MECP) optimization has been performed starting at the optimized non-CT S_1 minimum between the discontinuities in the central part of the PES cuts at the SF-DFT level to locate and investigate the CI. In both solvents, a CI could be identified with a dihedral angle of 103° lying structurally close to the isomerization coordinate. Due to almost degeneracy of S_0 and S_1 between the two discontinuities visible in Figure 5a and b, relaxation back to the electronic ground state can in principle occur at any point in this region. The molecular motion between the two discontinuities can be understood as a motion within the 3N-8 dimensional branching space of one CI. Since the *E*-isomer is formed when the excited molecules reach this CI and relax back to the ground state, this CI will be termed "productive" CI (CI_P) in the following. The productivity of this CI, however, also depends on whether the *Z* to *E* isomerization is completed in the ground state once the excited molecules reach it through the CI. This information is provided by the relaxed scans performed in the ground state. As can be seen from Figure 5c and d, the excited molecules must return to S_0 after the ground state barrier for the *Z* to *E* isomerization to be completed, i.e., at dihedral angles θ smaller than 80°, since they otherwise revert to the *Z*-isomer. Because in MeCN the CI is reached at an angle of 120°, while in benzene the CI is shifted toward a smaller angle of 100°, the excited molecules can relax back to the ground state earlier in more polar solvents. As a result, less molecules will isomerize to the *E* form in MeCN than in benzene once the productive CI_P is reached.

Due to the very fast unproductive relaxation in MeCN, a second unproductive CI is very likely to be present, possibly in the vicinity of the S_1 *Z*-minimum geometry. Another MECP optimization starting at the $S_{1,min}$ geometry did indeed reveal the presence of an additional CI, which lies energetically 0.35 and 0.5 eV above the S_1 *Z*-minimum in benzene and MeCN, respectively when the LR-PCM formalism is used. This represents an unproductive, immediate relaxation channel back to the S_0 *Z*-minimum, a so-called quenching CI (CI_Q). Since the energy difference between the CI and the S_1 minimum depends strongly on the stabilization of the latter by the solvent and LR-PCM is known to underestimate the latter, the energy difference computed by LR-PCM is certainly too small. A more reliable SS-PCM calculation is unfortunately not possible at the CI due to the degeneracy of the relevant states. Considering the excess energies of 0.20 and 1.32 eV and barrier heights larger than 0.35 and 0.5 eV in benzene and MeCN, respectively, this unproductive channel is energetically accessible only in polar environments.

Finally, we are now able to discuss the availability of the two competing relaxation channels involving either the productive or the quenching CI. The key quantity to consider is the excess energy, that is the energy available in the S_1 state for the molecules to perform reactions. In MeCN, the HTI molecules gain 1.32 eV of excess energy when relaxing from the Franck–Condon geometry to the S_1 *Z*-minimum, while in benzene they gain only as little as 0.2 eV. In MeCN, this energy is only sufficient to reach the quenching CI_Q at about 0.5 eV, which brings most of the excited state population back to the ground state, while the productive CI_P is unavailable due to a high isomerization barrier of 1.54 eV. Therefore, most of the excited state population should immediately relax through the quenching CI_Q. This is in line with the experimentally observed fast unproductive relaxation in MeCN. Furthermore, the productive CI_P is shifted toward more unfavorable dihedral angles in polar solvents, decreasing the probability of product formation in MeCN. Overall, the calculations show that in MeCN most of the excited state population is drained through a quenching channel, while product formation is barely possible.

Moving on to benzene, the excess energy is significantly reduced, preventing efficient relaxation through either of the CIs, independent of the chosen solvation model. Most of the population is thus trapped in the S_1 *Z*-minimum resulting in a significantly extended excited state lifetime. Since the barrier of 0.35 eV toward the quenching CI_Q only represents a lower boundary of the true barrier, it is not possible to identify a main decay channel in benzene solely from the quantum chemical calculations. However, according to the low combined quantum yield of ~10%, the quenching CI_Q should be at least as accessible as the productive CI_P. Overall, most of the excited state population relaxes back to the ground state without isomerization, while those few molecules that

https://doi.org/10.1021/jacs.3c03536
J. Am. Chem. Soc. 2023, 145, 14811−14822

eventually arrive at the productive CI_P most likely isomerize to the *E*-isomer.

Model of HTI Photodynamics. Overall, the findings of our quantum chemical calculations reproduce and explain the experimental data very well and allow us to construct a concise model for the ultrafast dynamics of the investigated sterically restricted HTI **1-A** (Figure 6). Following the excitation to the FC-region, the system relaxes quickly into the $S_{1,min}$. In contrast to the ground state S_0, the S_1 exhibits significant CT character. This is reflected by the solvent dependent stabilization of $S_{1,min}$ as evident by the strong red shift of the fluorescence with increasing polarity and supported by the calculated energies (Table 1). Due to the drastic change of the dipole moment between the S_0 and S_1, the solvent molecules reorganize on the few ps time scale causing shifts or small changes in the ESA intensity.

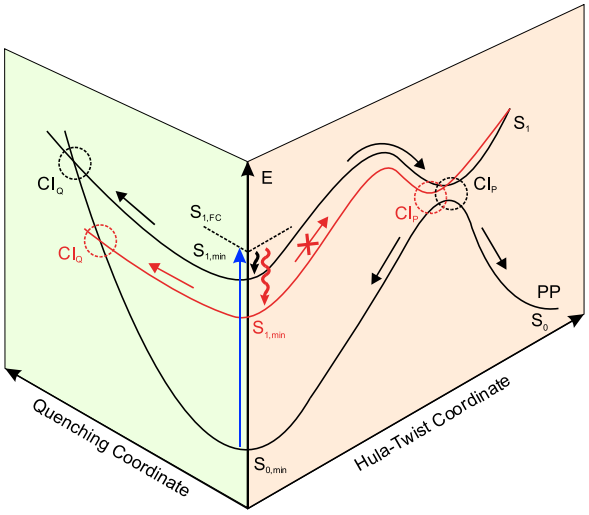

Figure 6. Schematic PES for the HTI **1-A** photoisomerization in benzene (black) and MeCN (red). Upon excitation to the FC-region (located at similar energies in both solvents) the excess energy in benzene is not sufficient to pass the barriers to the quenching CI (CI_Q) or productive CI (CI_P) immediately, trapping the molecule in the $S_{1,min}$. In MeCN, the excess energy is strongly increased due to the greater stabilization of $S_{1,min}$ with respect to $S_{1,FC}$, allowing fast relaxation through the accessible CI_Q. As the barrier to the CI_P possesses a lower dipole moment, it is less stabilized by MeCN and cannot be passed from the strongly stabilized $S_{1,min}$. In benzene, both CIs are accessible but only after passing significant barriers of similar height, which leads to the observed long excited state lifetime. Eventually, both CIs may be accessed, and photoproduct can be formed through the CI_P in contrast to MeCN and in agreement with the experimental quantum yields.

From the $S_{1,min}$ a barrier has to be overcome in all solvents to reach the CIs with the S_0 ground state based on the lifetimes in the range of tens to thousands of ps. The height of this barrier depends on the stabilization of the $S_{1,min}$ and the respective CI. Two CIs, a productive CI_P following a HT pathway and a quenching CI_Q exhibiting only small geometric changes with respect to the $S_{1,min}$ structure, determine the relaxation of the excited state population to the ground state. The accessibility of these CIs depends predominantly on the excess energy generated by relaxation from the FC-region and the barrier height to the CI.

In the case of the polar solvent MeCN, it can be concluded that the excess energy exceeds the barrier toward the quenching CI_Q in the excited state to explain the observed short excited state lifetime despite the uncertainty of the calculated barrier height. On the other hand, the high isomerization barrier prevents relaxation through the productive CI_P. In combination with the lower probability of product formation at the productive CI_P, this explains the vanishingly small quantum yields in MeCN.

In the apolar benzene, the excess energy is insufficient to immediately cross the barriers leading to vibrational cooling and the population being trapped in the S_1 minimum. This is in good agreement with the increased fluorescence intensities and excited state lifetimes observed in the TA. The excited state population is then drained through both the productive CI_P and quenching CI_Q where the ratio approximately correlates to the ratio of the barrier heights. Therefore, it is expected that the majority of the excited molecules undergo unproductive relaxation. However, those molecules accessing the productive CI_P most likely undergo efficient isomerization due to the more favorable location of the CI_P in apolar solvents reasonably explaining the observed low quantum yields. The finding that we do not observe distinct excited state populations that evolve separately indicates that the formation of photoproducts probably occurs on a shared pathway through the productive CI_P instead of distinct pathways with individual CIs as observed for other HTIs previously.[18,19] If one would assign the observed small excited state decay within tens to hundreds of ps to a distinct productive pathway, it would be expected that its ratio with the main decay correlates with the quantum yield if the solvent polarity is changed. A shared pathway seems plausible, due to the fact that the $S_{1,min}$ geometry already has significant resemblance and similar properties to a TICT state, which is typically the alternative relaxation pathway besides DBI.

It is likely that from the geometry of the productive CI_P relaxation via DBI or SBR is also possible instead of only forming the HT product. The distribution between these processes strongly depends on the exact landscape of the CI_P, which as we show in our calculations is strongly modified by the solvent polarity. The calculation of the direct SBR and DBI was not possible here, as the forced change of the appropriate coordinates would result in immediate steric clashes within the molecule due to significant steric constraints. Nevertheless, we were able to explain the different excited state lifetimes and investigated the quenching CI_Q, which should represent a competing relaxation channel for all three isomerization pathways.

CONCLUSION

In summary, our work provides first insights into the excited state dynamics and HT mechanism of a sterically restricted HTI by using a combination of ultrafast spectroscopy and quantum chemical calculations. We show that the HT photoreaction is a concerted process in which the central double bond and the adjacent single bond rotate concomitantly in the excited state to form the HT photoproduct. Due to large steric constraints and the presence of a strong electron-donating anilin fragment, the excited state lifetimes are extended and very sensitive to changes in solvent polarity. We assign this sensitivity to the strong CT character of the first excited state, which leads to significant modifications of the barrier height, excess energy in the excited state, and the resulting availability of alternative relaxation pathways. In contrast to other HTIs, we do not observe an obvious splitting

https://doi.org/10.1021/jacs.3c03536
J. Am. Chem. Soc. 2023, 145, 14811−14822

into different photoreaction pathways like DBI and TICT formation, as there is only one major excited state decay. This behavior is consistent throughout all three investigated solvents of different polarity even though the product yields and ratios change significantly. Therefore, we propose that in strongly constrained HTIs the product formation occurs on a shared pathway and splits into the individual product pathways from the same CI. The variation in solvent polarity might be enough to shift the PES landscape around the productive CI and modify the product ratios accordingly as evident by the solvent dependent shift of the productive CI in the theoretical description. The gained detailed insights thus lay the foundation for an atomistic understanding of the HT photoreaction and will aid future design and control of complex light-powered bond rotations in a fully conscious manner.

■ ASSOCIATED CONTENT

Supporting Information

The Supporting Information is available free of charge at https://pubs.acs.org/doi/10.1021/jacs.3c03536.

Details of synthesis, conformational analyses, photochemical, photophysical, and thermal behavior, quantum yield measurements, crystal structural data and calculated geometries of important structures as xyz-coordinates. (PDF)

Accession Codes

CCDC 2250057−2250060 contain the supplementary crystallographic data for this paper. These data can be obtained free of charge via www.ccdc.cam.ac.uk/data_request/cif, or by emailing data_request@ccdc.cam.ac.uk, or by contacting The Cambridge Crystallographic Data Centre, 12 Union Road, Cambridge CB2 1EZ, UK; fax: +44 1223 336033.

■ AUTHOR INFORMATION

Corresponding Authors

Andreas Dreuw − *Interdisciplinary Center for Scientific Computing, Ruprecht-Karls University Heidelberg, 69120 Heidelberg, Germany*; Email: dreuw@uni-heidelberg.de

Henry Dube − *Department of Chemistry and Pharmacy, Friedrich-Alexander University Erlangen-Nürnberg, 91058 Erlangen, Germany*; orcid.org/0000-0002-5055-9924; Email: henry.dube@fau.de

Josef Wachtveitl − *Institute of Physical and Theoretical Chemistry, Goethe University Frankfurt am Main, 60438 Frankfurt, Germany*; orcid.org/0000-0002-8496-8240; Email: wveitl@theochem.uni-frankfurt.de

Authors

Tobias Fischer − *Institute of Physical and Theoretical Chemistry, Goethe University Frankfurt am Main, 60438 Frankfurt, Germany*; orcid.org/0000-0002-4196-5509

Jonas Leitner − *Interdisciplinary Center for Scientific Computing, Ruprecht-Karls University Heidelberg, 69120 Heidelberg, Germany*

Aaron Gerwien − *Department of Chemistry and Center for Integrated Protein Science CIPSM, Ludwig-Maximilians Universität München, 81377 Munich, Germany*

Peter Mayer − *Department of Chemistry and Center for Integrated Protein Science CIPSM, Ludwig-Maximilians Universität München, 81377 Munich, Germany*

Complete contact information is available at: https://pubs.acs.org/10.1021/jacs.3c03536

Author Contributions

⊥These authors contributed equally.

Notes

The authors declare no competing financial interest.

■ ACKNOWLEDGMENTS

H.D. thanks the Deutsche Forschungsgemeinschaft (DFG) for an Emmy Noether fellowship (DU 1414/1-2). J.W. acknowledges the DFG (WA 1850/4-3) for funding. J.L. acknowledges funding of the DFG through the research training group CLiC (GRK 1986, Complex Light-Control). This project has also received funding from the European Research Council (ERC) under the European Union's Horizon 2020 research and innovation programme (PHOTOMECH, grant agreement No. 101001794).

■ ABBREVIATIONS

cHex, cyclohexane; CI, conical intersection; CT, charge transfer; DAS, decay-associated spectra; DBI, double bond isomerization; ESA, excited state absorption; GSB, ground state bleach; GTA, global target analysis; HT, Hula-Twist; HTI, hemithioindigo; LR-PCM, linear response polarizable continuum model; MeCN, acetonitrile; MECP, minimum energy crossing point; NOPA, noncollinear optical parametric amplifier; NTO, natural transition orbital; OD, optical density; PES, Potential energy surface; SBR, single bond rotation; SBT, single bond twisting; SE, stimulated emission; SF-DFT, Spin-flip density functional theory; SS-PCM, state specific polarizable continuum model; TA, transient absorption; TDA, Tamm-Dancoff approximation; TD-DFT, Time-dependent density functional theory; TICT, Twisted intramolecular charge transfer

■ REFERENCES

(1) Cordes, T.; Weinrich, D.; Kempa, S.; Riesselmann, K.; Herre, S.; Hoppmann, C.; Rück-Braun, K.; Zinth, W. Hemithioindigo-Based Photoswitches as Ultrafast Light Trigger in Chromopeptides. *Chem. Phys. Lett.* **2006**, *428* (1−3), 167−173.

(2) Cordes, T.; Schadendorf, T.; Rück-Braun, K.; Zinth, W. Chemical Control of Hemithioindigo-Photoisomerization - Substituent-Effects on Different Molecular Parts. *Chem. Phys. Lett.* **2008**, *455* (4−6), 197−201.

(3) Cordes, T.; Schadendorf, T.; Priewisch, B.; Rück-Braun, K.; Zinth, W. The Hammett Relationship and Reactions in the Excited Electronic State: Hemithioindigo Z/E-Photoisomerization. *J. Phys. Chem. A* **2008**, *112* (4), 581−588.

(4) Nenov, A.; Cordes, T.; Herzog, T. T.; Zinth, W.; De Vivie-Riedle, R. Molecular Driving Forces for Z/E Isomerization Mediated by Heteroatoms: The Example Hemithioindigo. *J. Phys. Chem. A* **2010**, *114* (50), 13016−13030.

(5) Maerz, B.; Wiedbrauk, S.; Oesterling, S.; Samoylova, E.; Nenov, A.; Mayer, P.; De Vivie-Riedle, R.; Zinth, W.; Dube, H. Making Fast Photoswitches Faster - Using Hammett Analysis to Understand the Limit of Donor-Acceptor Approaches for Faster Hemithioindigo Photoswitches. *Chem. - Eur. J.* **2014**, *20* (43), 13984−13992.

(6) Wiedbrauk, S.; Dube, H. Hemithioindigo-An Emerging Photoswitch. *Tetrahedron Lett.* **2015**, *56* (29), 4266−4274.

(7) Regner, N.; Herzog, T. T.; Haiser, K.; Hoppmann, C.; Beyermann, M.; Sauermann, J.; Engelhard, M.; Cordes, T.; Rück-Braun, K.; Zinth, W. Light-Switchable Hemithioindigo-Hemistilbene-Containing Peptides: Ultrafast Spectroscopy of the Z → e Isomerization of the Chromophore and the Structural Dynamics of the Peptide Moiety. *J. Phys. Chem. B* **2012**, *116* (14), 4181−4191.

(8) Füllbeck, M.; Michalsky, E.; Jaeger, I. S.; Henklein, P.; Kuhn, H.; Rück-Braun, K.; Preissner, R. Design and Biological Evaluation of Photo-Switchable Inhibitors. *Genome Inform. Int. Conf. Genome Inform.* **2006**, *17* (1), 141−151.
(9) Eggers, K.; Fyles, T. M.; Montoya-Pelaez, P. J. Synthesis and Characterization of Photoswitchable Lipids Containing Hemithioindigo Chromophores. *J. Org. Chem.* **2001**, *66* (9), 2966−2977.
(10) Kitzig, S.; Thilemann, M.; Cordes, T.; Rück-Braun, K. Light-Switchable Peptides with a Hemithioindigo Unit: Peptide Design, Photochromism, and Optical Spectroscopy. *ChemPhysChem* **2016**, *17* (9), 1252−1263.
(11) Tanaka, K.; Taguchi, K.; Iwata, S.; Irie, T. Application of Benzoyl-Substituted Hemithioindigo as a Molecular Switch in Porphyrin-Quinone Recognition. *Supramol. Chem.* **2005**, *17* (8), 637−642.
(12) Tanaka, K.; Kohayakawa, K.; Iwata, S.; Irie, T. Application of 2-Pyridyl-Substituted Hemithioindigo as a Molecular Switch in Hydrogen-Bonded Porphyrins. *J. Org. Chem.* **2008**, *73* (10), 3768−3774.
(13) Dube, H.; Rebek, J. Selective Guest Exchange in Encapsulation Complexes Using Light of Different Wavelenghts. *Angew. Chem. - Int. Ed.* **2012**, *51* (13), 3207−3210.
(14) Guentner, M.; Uhl, E.; Mayer, P.; Dube, H. Photocontrol of Polar Aromatic Interactions by a Bis-Hemithioindigo Based Helical Receptor. *Chem. - Eur. J.* **2016**, *22* (46), 16433−16436.
(15) Guentner, M.; Schildhauer, M.; Thumser, S.; Mayer, P.; Stephenson, D.; Mayer, P. J.; Dube, H. Sunlight-Powered kHz Rotation of a Hemithioindigo-Based Molecular Motor. *Nat. Commun.* **2015**, *6* (1), 8406.
(16) Stallhofer, K.; Nuber, M.; Schüppel, F.; Thumser, S.; Iglev, H.; De Vivie-Riedle, R.; Zinth, W.; Dube, H. Electronic and Geometric Characterization of TICT Formation in Hemithioindigo Photoswitches by Picosecond Infrared Spectroscopy. *J. Phys. Chem. A* **2021**, *125* (20), 4390−4400.
(17) Gerwien, A.; Schildhauer, M.; Thumser, S.; Mayer, P.; Dube, H. Direct Evidence for Hula Twist and Single-Bond Rotation Photoproducts. *Nat. Commun.* **2018**, *9* (1), 2510.
(18) Wiedbrauk, S.; Maerz, B.; Samoylova, E.; Mayer, P.; Zinth, W.; Dube, H. Ingredients to TICT Formation in Donor Substituted Hemithioindigo. *J. Phys. Chem. Lett.* **2017**, *8* (7), 1585−1592.
(19) Wiedbrauk, S.; Maerz, B.; Samoylova, E.; Reiner, A.; Trommer, F.; Mayer, P.; Zinth, W.; Dube, H. Twisted Hemithioindigo Photoswitches: Solvent Polarity Determines the Type of Light-Induced Rotations. *J. Am. Chem. Soc.* **2016**, *138* (37), 12219−12227.
(20) Gerwien, A.; Reinhardt, T.; Mayer, P.; Dube, H. Synthesis of Double-Bond-Substituted Hemithioindigo Photoswitches. *Org. Lett.* **2018**, *20* (1), 232−235.
(21) Köttner, L.; Schildhauer, M.; Wiedbrauk, S.; Mayer, P.; Dube, H. Oxidized Hemithioindigo Photoswitches—Influence of Oxidation State on (Photo)Physical and Photochemical Properties. *Chem. - Eur. J.* **2020**, *26* (47), 10712−10718.
(22) Liu, R. S.; Asato, A. E. The Primary Process of Vision and the Structure of Bathorhodopsin: A Mechanism for Photoisomerization of Polyenes. *Proc. Natl. Acad. Sci. U. S. A.* **1985**, *82* (2), 259−263.
(23) Fuß, W.; Kosmidis, C.; Schmid, W. E.; Trushin, S. A. The Photochemical Cis-Trans Isomerization of Free Stilbene Molecules Follows a Hula-Twist Pathway. *Angew. Chem. - Int. Ed.* **2004**, *43* (32), 4178−4182.
(24) Warshel, A. Bicycle-Pedal Model for the First Step in the Vision Process. *Nature* **1976**, *260* (5553), 679−683.
(25) Gerwien, A.; Mayer, P.; Dube, H. Photon-Only Molecular Motor with Reverse Temperature-Dependent Efficiency. *J. Am. Chem. Soc.* **2018**, *140* (48), 16442−16446.
(26) Gerwien, A.; Jehle, B.; Irmler, M.; Mayer, P.; Dube, H. An Eight-State Molecular Sequential Switch Featuring a Dual Single-Bond Rotation Photoreaction. *J. Am. Chem. Soc.* **2022**, *144* (7), 3029−3038.
(27) Imamoto, Y.; Kuroda, T.; Kataoka, M.; Shevyakov, S.; Krishnamoorthy, G.; Liu, R. S. H. Photoisomerization by Hula Twist: 2,2′-Dimethylstilbene and a Ring-Fused Analogue. *Angew. Chem., Int. Ed.* **2003**, *42* (31), 3630−3633.
(28) Müller, A. M.; Lochbrunner, S.; Schmid, W. E.; Fuß, W. Low-Temperature Photochemistry of Previtamin D: A Hula-Twist Isomerization of a Triene. *Angew. Chem., Int. Ed.* **1998**, *37* (4), 505−507.
(29) Maessen, P. A.; Jacobs, H. J. C.; Cornelisse, J.; Havinga, E. Photochemistry of Previtamin D3 at 92 K; Formation of an Unstable Tachysterol3 Rotamer. *Angew. Chem., Int. Ed.* **1983**, *22* (9), 718−719.
(30) Saltiel, J.; Megarity, E. D.; Kneipp, K. G. The Mechanism of Direct Cis-Trans Photoisomerization of the Stilbenes. *J. Am. Chem. Soc.* **1966**, *88* (10), 2336−2338.
(31) Bayda, M.; Redwood, C. E.; Gupta, S.; Dmitrenko, O.; Saltiel, J. Lumisterol to Tachysterol Photoisomerization in EPA Glass at 77 K. A Comparative Study. *J. Phys. Chem. A* **2017**, *121* (12), 2331−2342.
(32) Redwood, C.; Bayda, M.; Saltiel, J. Photoisomerization of Pre- and Provitamin D3 in EPA at 77 K: One-Bond-Twist, Not Hula-Twist. *J. Phys. Chem. Lett.* **2013**, *4* (5), 716−721.
(33) Jung, Y. O.; Lee, J. H.; Kim, J.; Schmidt, M.; Moffat, K.; Šrajer, V.; Ihee, H. Volume-Conserving Trans−Cis Isomerization Pathways in Photoactive Yellow Protein Visualized by Picosecond X-Ray Crystallography. *Nat. Chem.* **2013**, *5* (3), 212−220.
(34) Kaila, V. R. I.; Schotte, F.; Cho, H. S.; Hummer, G.; Anfinrud, P. A. Contradictions in X-Ray Structures of Intermediates in the Photocycle of Photoactive Yellow Protein. *Nat. Chem.* **2014**, *6* (4), 258−259.
(35) Jung, Y. O.; Lee, J. H.; Kim, J.; Schmidt, M.; Moffat, K.; Šrajer, V.; Ihee, H. Reply to "Contradictions in X-Ray Structures of Intermediates in the Photocycle of Photoactive Yellow Protein. *Nat. Chem.* **2014**, *6* (4), 259−260.
(36) Slavov, C.; Bellakbil, N.; Wahl, J.; Mayer, K.; Rück-Braun, K.; Burghardt, I.; Wachtveitl, J.; Braun, M. Ultrafast Coherent Oscillations Reveal a Reactive Mode in the Ring-Opening Reaction of Fulgides. *Phys. Chem. Chem. Phys.* **2015**, *17*, 14045−14053.
(37) Slavov, C.; Hartmann, H.; Wachtveitl, J. Implementation and Evaluation of Data Analysis Strategies for Time-Resolved Optical Spectroscopy. *Anal. Chem.* **2015**, *87* (4), 2328−2336.
(38) Frisch, M. J.; Trucks, G. W.; Schlegel, H. B.; Scuseria, G. E.; Robb, M. a.; Cheeseman, J. R.; Scalmani, G.; Barone, V.; Petersson, G. A.; Nakatsuji, H.; Li, X.; Caricato, M.; Marenich, A. V.; Bloino, J.; Janesko, B. G.; Gomperts, R.; Mennucci, B.; Hratchian, H. P.; Ortiz, J. V.; Izmaylov, A. F.; Sonnenberg, J. L.; Williams-Young, D.; Ding, F.; Lipparini, F.; Egidi, F.; Goings, J.; Peng, B.; Petrone, A.; Henderson, T.; Ranasinghe, D.; Zakrzewski, V. G.; Gao, J.; Rega, N.; Zheng, G.; Liang, W.; Hada, M.; Ehara, M.; Toyota, K.; Fukuda, R.; Hasegawa, J.; Ishida, M.; Nakajima, T.; Honda, Y.; Kitao, O.; Nakai, H.; Vreven, T.; Throssell, K.; Montgomery, J. A., Jr.; Peralta, J. E.; Ogliaro, F.; Bearpark, M. J.; Heyd, J. J.; Brothers, E. N.; Kudin, K. N.; Staroverov, V. N.; Keith, T. A.; Kobayashi, R.; Normand, J.; Raghavachari, K.; Rendell, A. P.; Burant, J. C.; Iyengar, S. S.; Tomasi, J.; Cossi, M.; Millam, J. M.; Klene, M.; Adamo, C.; Cammi, R.; Ochterski, J. W.; Martin, R. L.; Morokuma, K.; Farkas, O.; Foresman, J. B.; Fox, D. J. *Gaussian 16*, Revision B.01; Gaussian, Inc.: Wallingford, CT, 2016.
(39) Parr, R. G. In *Density Functional Theory of Atoms and Molecules BT - Horizons of Quantum Chemistry*; Fukui, K., Pullman, B., Eds.; Springer Netherlands: Dordrecht, 1980; pp 5−15.
(40) Yanai, T.; Tew, D. P.; Handy, N. C. A New Hybrid Exchange-Correlation Functional Using the Coulomb-Attenuating Method (CAM-B3LYP). *Chem. Phys. Lett.* **2004**, *393* (1−3), 51−57.
(41) Scalmani, G.; Frisch, M. J. Continuous Surface Charge Polarizable Continuum Models of Solvation. I. General Formalism. *J. Chem. Phys.* **2010**, *132* (11), 114110.
(42) Dreuw, A.; Head-Gordon, M. Single-Reference Ab Initio Methods for the Calculation of Excited States of Large Molecules. *Chem. Rev.* **2005**, *105* (11), 4009−4037.
(43) Epifanovsky, E.; Gilbert, A. T. B.; Feng, X.; Lee, J.; Mao, Y.; Mardirossian, N.; Pokhilko, P.; White, A. F.; Coons, M. P.; Dempwolff, A. L.; Gan, Z.; Hait, D.; Horn, P. R.; Jacobson, L. D.; Kaliman, I.; Kussmann, J.; Lange, A. W.; Lao, K. U.; Levine, D. S.; Liu,

https://doi.org/10.1021/jacs.3c03536
J. Am. Chem. Soc. 2023, 145, 14811−14822

J.; McKenzie, S. C.; Morrison, A. F.; Nanda, K. D.; Plasser, F.; Rehn, D. R.; Vidal, M. L.; You, Z. Q.; Zhu, Y.; Alam, B.; Albrecht, B. J.; Aldossary, A.; Alguire, E.; Andersen, J. H.; Athavale, V.; Barton, D.; Begam, K.; Behn, A.; Bellonzi, N.; Bernard, Y. A.; Berquist, E. J.; Burton, H. G. A.; Carreras, A.; Carter-Fenk, K.; Chakraborty, R.; Chien, A. D.; Closser, K. D.; Cofer-Shabica, V.; Dasgupta, S.; De Wergifosse, M.; Deng, J.; Diedenhofen, M.; Do, H.; Ehlert, S.; Fang, P. T.; Fatehi, S.; Feng, Q.; Friedhoff, T.; Gayvert, J.; Ge, Q.; Gidofalvi, G.; Goldey, M.; Gomes, J.; González-Espinoza, C. E.; Gulania, S.; Gunina, A. O.; Hanson-Heine, M. W. D.; Harbach, P. H. P.; Hauser, A.; Herbst, M. F.; Hernández Vera, M.; Hodecker, M.; Holden, Z. C.; Houck, S.; Huang, X.; Hui, K.; Huynh, B. C.; Ivanov, M.; Jász, Á.; Ji, H.; Jiang, H.; Kaduk, B.; Kähler, S.; Khistyaev, K.; Kim, J.; Kis, G.; Klunzinger, P.; Koczor-Benda, Z.; Koh, J. H.; Kosenkov, D.; Koulias, L.; Kowalczyk, T.; Krauter, C. M.; Kue, K.; Kunitsa, A.; Kus, T.; Ladjánszki, I.; Landau, A.; Lawler, K. V.; Lefrancois, D.; Lehtola, S.; Li, R. R.; Li, Y. P.; Liang, J.; Liebenthal, M.; Lin, H. H.; Lin, Y. S.; Liu, F.; Liu, K. Y.; Loipersberger, M.; Luenser, A.; Manjanath, A.; Manohar, P.; Mansoor, E.; Manzer, S. F.; Mao, S. P.; Marenich, A. V.; Markovich, T.; Mason, S.; Maurer, S. A.; McLaughlin, P. F.; Menger, M. F. S. J.; Mewes, J. M.; Mewes, S. A.; Morgante, P.; Mullinax, J. W.; Oosterbaan, K. J.; Paran, G.; Paul, A. C.; Paul, S. K.; Pavošević, F.; Pei, Z.; Prager, S.; Proynov, E. I.; Rák, Á.; Ramos-Cordoba, E.; Rana, B.; Rask, A. E.; Rettig, A.; Richard, R. M.; Rob, F.; Rossomme, E.; Scheele, T.; Scheurer, M.; Schneider, M.; Sergueev, N.; Sharada, S. M.; Skomorowski, W.; Small, D. W.; Stein, C. J.; Su, Y. C.; Sundstrom, E. J.; Tao, Z.; Thirman, J.; Tornai, G. J.; Tsuchimochi, T.; Tubman, N. M.; Veccham, S. P.; Vydrov, O.; Wenzel, J.; Witte, J.; Yamada, A.; Yao, K.; Yeganeh, S.; Yost, S. R.; Zech, A.; Zhang, I. Y.; Zhang, X.; Zhang, Y.; Zuev, D.; Aspuru-Guzik, A.; Bell, A. T.; Besley, N. A.; Bravaya, K. B.; Brooks, B. R.; Casanova, D.; Chai, J.; Da; Coriani, S.; Cramer, C. J.; Cserey, G.; Deprince, A. E.; Distasio, R. A.; Dreuw, A.; Dunietz, B. D.; Furlani, T. R.; Goddard, W. A.; Hammes-Schiffer, S.; Head-Gordon, T.; Hehre, W. J.; Hsu, C. P.; Jagau, T. C.; Jung, Y.; Klamt, A.; Kong, J.; Lambrecht, D. S.; Liang, W.; Mayhall, N. J.; McCurdy, C. W.; Neaton, J. B.; Ochsenfeld, C.; Parkhill, J. A.; Peverati, R.; Rassolov, V. A.; Shao, Y.; Slipchenko, L. V.; Stauch, T.; Steele, R. P.; Subotnik, J. E.; Thom, A. J. W.; Tkatchenko, A.; Truhlar, D. G.; Van Voorhis, T.; Wesolowski, T. A.; Whaley, K. B.; Woodcock, H. L.; Zimmerman, P. M.; Faraji, S.; Gill, P. M. W.; Head-Gordon, M.; Herbert, J. M.; Krylov, A. I. Software for the Frontiers of Quantum Chemistry: An Overview of Developments in the Q-Chem 5 Package. *J. Chem. Phys.* **2021**, *155* (8), 084801.

(44) Shao, Y.; Head-Gordon, M.; Krylov, A. I. The Spin-Flip Approach within Time-Dependent Density Functional Theory: Theory and Applications to Diradicals. *J. Chem. Phys.* **2003**, *118* (11), 4807−4818.

(45) Hirata, S.; Head-Gordon, M. Time-Dependent Density Functional Theory within the Tamm-Dancoff Approximation. *Chem. Phys. Lett.* **1999**, *314* (3−4), 291−299.

(46) Graupner, F. F.; Herzog, T. T.; Rott, F.; Oesterling, S.; de Vivie-Riedle, R.; Cordes, T.; Zinth, W. Photoisomerization of Hemithioindigo Compounds: Combining Solvent- and Substituent-Effects into an Advanced Reaction Model. *Chem. Phys.* **2018**, *515*, 614−621.

(47) Plötner, J.; Dreuw, A. Molecular Mechanism of the Z/E-Photoisomerization of Hemithioindigo Hemistilbene. *J. Phys. Chem. A* **2009**, *113* (43), 11882−11887.

(48) Corni, S.; Cammi, R.; Mennucci, B.; Tomasi, J. Electronic Excitation Energies of Molecules in Solution within Continuum Solvation Models: Investigating the Discrepancy between State-Specific and Linear-Response Methods. *J. Chem. Phys.* **2005**, *123* (13), 134512.

https://doi.org/10.1021/jacs.3c03536
J. Am. Chem. Soc. 2023, 145, 14811−14822